

## Article

# Porous Electrodeposited Cu as a Potential Electrode for Electrochemical Reduction Reactions of CO<sub>2</sub>

Jidsucha Darayen <sup>1</sup>, Orawon Chailapakul <sup>2</sup>, Piyan Praserthdam <sup>3</sup>, Joongjai Panpranot <sup>4</sup>, Duangamol N. Tungasmita <sup>5</sup>  and Yuttanant Boonyongmaneerat <sup>6,\*</sup>

<sup>1</sup> Nanoscience and Technology Interdisciplinary Program, Graduate School, Chulalongkorn University, Bangkok 10330, Thailand; d.jidsucha@gmail.com

<sup>2</sup> Electrochemistry and Optical Spectroscopy Center of Excellence (EOSCE), Chulalongkorn University, Bangkok 10330, Thailand; corawon@chula.ac.th

<sup>3</sup> Department of Chemical Engineering, Faculty of Engineering, Chulalongkorn University, Bangkok 10330, Thailand; piyasan.p@chula.ac.th

<sup>4</sup> Center of Excellence on Catalysis and Catalytic Reaction Engineering (CECC), Chulalongkorn University, Bangkok 10330, Thailand; joongjai.p@chula.ac.th

<sup>5</sup> Green Chemistry for Fine Chemical Productions STAR, Department of Chemistry, Faculty of Science, Chulalongkorn University, Bangkok 10330, Thailand; duangamol.n@chula.ac.th

<sup>6</sup> Surface Coatings Technology for Metals and Materials Research Unit, Metallurgy and Materials Science Research Institute, Chulalongkorn University, Bangkok 10330, Thailand

\* Correspondence: yuttanant.b@chula.ac.th



**Citation:** Darayen, J.; Chailapakul, O.; Praserthdam, P.; Panpranot, J.; Tungasmita, D.N.; Boonyongmaneerat, Y. Porous Electrodeposited Cu as a Potential Electrode for Electrochemical Reduction Reactions of CO<sub>2</sub>. *Appl. Sci.* **2021**, *11*, 11104. <https://doi.org/10.3390/app112311104>

Academic Editor: Valentina Belova

Received: 8 October 2021

Accepted: 17 November 2021

Published: 23 November 2021

**Publisher's Note:** MDPI stays neutral with regard to jurisdictional claims in published maps and institutional affiliations.



**Copyright:** © 2021 by the authors. Licensee MDPI, Basel, Switzerland. This article is an open access article distributed under the terms and conditions of the Creative Commons Attribution (CC BY) license (<https://creativecommons.org/licenses/by/4.0/>).

**Abstract:** In the present study, a systematic investigation is performed to assess the relationship between electroplating parameters, pore morphology and internal surface area of copper deposits which are promising to serve as electrodes for electrochemical reduction reactions of carbon dioxide (CO<sub>2</sub>). A set of porous copper deposits are fabricated with the dynamic hydrogen bubble template method. The microstructural and Brunauer–Emmett–Teller (BET) analysis demonstrate that current density, deposition time, and bath composition control pore size, strut size, and hence surface area which could be as high as 20 m<sup>2</sup>/g. Selected sets of porous copper electrodes are then employed in the electrochemical reduction reaction test to determine their conversion performance in comparison to a monolithic copper surface. From the gas chromatography (GC) and nuclear magnetic resonance (NMR) analysis, porous copper is shown to provide higher rates of production of some important chemicals, as compared to copper foil electrodes. Porous copper with fern-like morphology serves as a promising electrode that yields relatively high amounts of acetaldehyde, acetate and ethanol. The study thus presents the opportunities to enhance the electrochemical reduction reaction of CO<sub>2</sub> through microstructural engineering of the copper surface, which benefits both CO<sub>2</sub> reduction and generation of chemical products of high value.

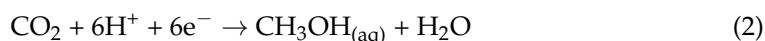
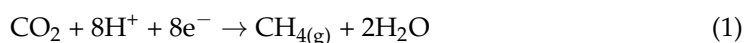
**Keywords:** porous copper; electrochemical CO<sub>2</sub> reduction; catalyst; surface microstructure

## 1. Introduction

High attention has been paid to the development of porous metals in the past decade, because the materials exhibit many unique characteristics including high surface area, low density, and permeability that allow fluid flow. Recently, porous copper (Cu) and Cu alloys are among the porous metals that receive increasing focus, as Cu itself provides many important features required in the engineering and functional applications [1–5]. These include, for example, high thermal conductivity for heat exchangers and catalytic activity for environmental and energy applications [6–8]. Introduction of porosity to Cu has been shown to enhance various properties, such as wettability, fluid permeability and catalytic efficiency [9–12]. Correspondingly, Cu with porous structures, coupled with its metallic copper quality, can find wider uses for thermal transfer systems, water purification, fuel cell components and electro-catalytic applications [13–17].

One of the possible techniques to generate porosity and thus fabricate porous Cu is the promotion of hydrogen bubbles in the Cu electrodeposition process in the acid-based electrolyte. This so-called “dynamic hydrogen bubble template (DHBT) method” was introduced by Shin et al. in the year 2003 and was demonstrated to provide honeycomb-like porous structure with hierarchical porosity, comprising pores in micro- (30–90  $\mu\text{m}$ ) and nano-scales [4,18]. Specifically, porosity can be generated in a relatively simple way by increasing the rates of hydrogen formation at the cathode surface upon which Cu ions are electrochemically reduced and copper is electrodeposited. This could be done by increasing applied current for electrodeposition or increasing the concentration ratio of sulfuric acid to copper sulphate in the plating bath [4,18–21]. The accumulated hydrogen bubbles are then incorporated into the deposit, resulting in pore formation.

With high volume of interconnected porosity and large surface area, DHBT porous Cu can find possible uses in the application of electrochemical  $\text{CO}_2$  reduction reactions ( $\text{CO}_2\text{RR}$ ), as an electro-catalyst that supports and accelerates the conversion of  $\text{CO}_2$  gas to some useful chemical products [2,10,22,23]. This particular application has gained large amounts of attention in recent years owing to the increasing concern on greenhouse gas emissions and associated global warming. Compared to the existing thermochemical, photochemical, and hydrogenation methods, the electrochemical route for  $\text{CO}_2$  conversion is advantageous due to its low energy consumption, dispatchability and room temperature operation [24]. In this regard, the 3D open-pore catalytic electrode of high surface could allow  $\text{CO}_2$  to concentrate at the electrode and provide more active sites for the electrochemical reaction [1,2]. Compared to other common electrodes for  $\text{CO}_2\text{RR}$  (e.g., Au, Ag and Zn that provide CO primarily; and Sn, In, Pb that dominantly yield formate) [25,26], Cu is known to be a unique catalyst that promote generations of a variety of valuable chemical products, including CO, formate, hydrocarbons (i.e., methane, ethylene, and ethane), and oxygenates (i.e., acetate, acetone, ethanol, formate, and methanol) [6,25–29]. A state-of-the-art study by Kuhl et al. using a flat cell reactor and Cu foil electrodes demonstrated the generation of as many as 16  $\text{CO}_2\text{RR}$  products [26], owing to Cu’s intermediate CO binding energy. Oxidation states of Cu electrodes’ surfaces (i.e.,  $\text{Cu}^+$ ,  $\text{Cu}^{2+}$ ) have shown to play a role in  $\text{CO}_2\text{RR}$ . Depending on the oxidation states as controllable by various methods [30] such as thermal annealing, Cu electrodes are promoted to generate different chemical products and current efficiencies [31–34]. Of the primary uses of Cu electro-catalysts for  $\text{CO}_2$  conversion applications are those that produce hydrocarbon or oxygenate products [10,25], as exemplified by the cathodic electrochemical reactions in Equations (1) and (2). The anodic reactions, on the other hand, involve the oxygen evolution reaction (OER), whereby oxygen molecules and electrons are generated at the anodes.



Compared to monolithic Cu electrodes, porous Cu electrodes could potentially contribute to improvements of product selectivity, catalytic activity, and energy consumption of  $\text{CO}_2\text{RR}$ . Nevertheless, a study of porous Cu or porous metals in general for the  $\text{CO}_2\text{RR}$  application is still limited. Daiyan et al., for example, demonstrated that introduction of porosity with a certain pore size to Ag deposits results in the increase of faradaic efficiency for  $\text{CO}_2$  conversion to CO [35]. Palmore et al. introduced DHBT Cu for  $\text{CO}_2\text{RR}$  and showed that the porous Cu that was deposited with a certain duration (i.e., 60 s) preferably enhances faradic efficiency of hydrocarbons (methane, ethylene, and propene) [10]. Nam et al. recently studied the influence of pore morphology of Cu electrodes, particularly the width and depth of pores, on  $\text{CO}_2\text{RR}$ . The group showed that it largely affects product distributions of hydrogen ( $\text{H}_2$ ), ethylene ( $\text{CH}_4$ ), and ethane ( $\text{CH}_6$ ) [22]. Likewise, Dutta et al. demonstrated that surface modification of porous Cu electrodes could further influence  $\text{CO}_2\text{RR}$  product distribution [2].

## 2. Materials and Methods

### 2.1. Sample Fabrication

Three groups of porous Cu samples, to be named A, B, and C, were fabricated by the process of Cu electrodeposition onto high-purity copper foils (0.1 mm thick, 99.9999% purity (Alfa Aesar)) with a dimension of 2.5 cm × 2.5 cm. The three groups differ from one another by the compositions of H<sub>2</sub>SO<sub>4</sub>, CuSO<sub>4</sub> and HCl in the plating solutions (300 cc), as shown in Table 1. A standard setup of electrodeposition of Cu was employed at room temperature (28 °C), using platinum mesh as an anode. Prior to running the reaction, a Cu foil was dipped in 5% H<sub>2</sub>SO<sub>4</sub> for 10 s. For each of the sample groups, the deposition was performed by varying applied current density (2, 3, and 3.5 A/cm<sup>2</sup>), and deposition time (20, 40 and 60 s), resulting in nine sub-sets of samples for each group.

**Table 1.** Electrodeposition parameters employed for fabrication of the porous Cu electrodes.

Sample Group	Bath Composition	Current Density (A/cm <sup>2</sup> )	Deposition Time (s)
A	1.5M H <sub>2</sub> SO <sub>4</sub> + 0.2M CuSO <sub>4</sub>	2, 3, 3.5	20, 40, 60
B	1.5M H <sub>2</sub> SO <sub>4</sub> + 0.4M CuSO <sub>4</sub>	2, 3, 3.5	20, 40, 60
C	1.5M H <sub>2</sub> SO <sub>4</sub> + 0.4M CuSO <sub>4</sub> + 0.05M HCl	2, 3, 3.5	20, 40, 60

### 2.2. Sample Characterization

The Cu deposit samples were subsequently analyzed for their physical and chemical characteristics. Surface morphology was investigated by optical and scanning electron microscopy (OM and SEM (15 kV)). Apparent pore size and apparent porosity, representing 2D-pore characteristics, were analyzed from micrographs using Image J software. True surface area, representing the surface area of 3D structures, was determined by BET technique (degassing at 200 °C by nitrogen gas flow for 5 h). Moreover, true porosity, representing an actual percentage of pore in a given volume, can be calculated with Equation (3). Energy dispersive X-ray (EDX) and X-ray photoelectron spectroscopy (XPS) analysis was used to confirm the chemical composition on the surface.

$$\text{True porosity} = \left( 1 - \frac{\text{apparent density of sample}}{\text{density of metal}} \right) \times 100 \quad (3)$$

### 2.3. CO<sub>2</sub>RR Experiment

Three sets of porous Cu samples from A, B and C sample groups, electrodeposited with 3 A/cm<sup>2</sup> for 40 s, were chosen as working electrodes for CO<sub>2</sub>RR tests. The electrochemical CO<sub>2</sub>RR process was conducted using a 3-electrode H-cell setup, consisting of a working electrode (WE: Cu deposit samples), a counter electrode (CE: platinum foil), and a reference electrode (RE: Ag/AgCl). The cathodic and anodic compartments were separated by Nafion 117 membrane. Potassium bicarbonate (KHCO<sub>3</sub>) with concentration and volume of 0.1 M and 40 cc was used as the electrolyte. A schematic picture of the setup is illustrated in Figure 1. Before each test session, high purity (99.9%) CO<sub>2</sub> was purged into the cell for 60 min. Once the pH level of the electrolyte changed from 8.2 to 6.8, the test session was initiated. CO<sub>2</sub> was purged continuously during the test, and the cell was applied with a voltage of −1.3 V vs. Ag/AgCl.

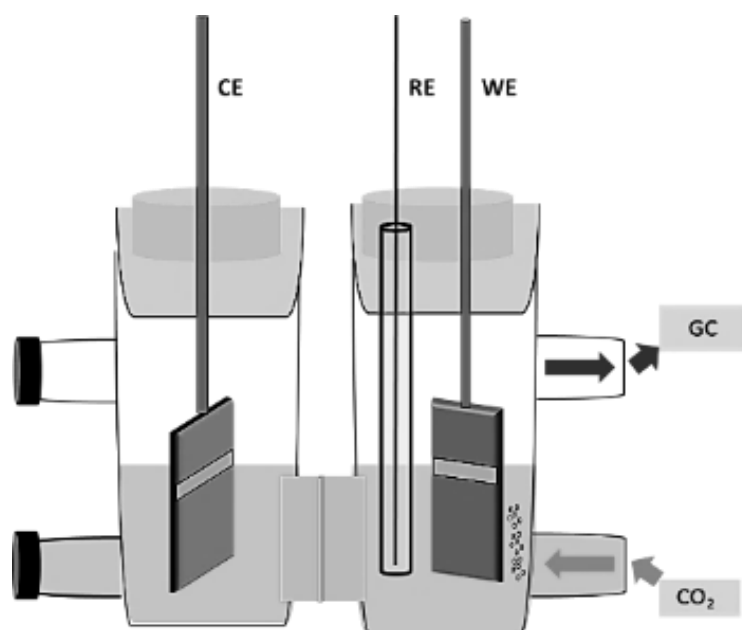


**Figure 1.** Schematic of a 3-electrode H-cell setup for the CO<sub>2</sub> reduction reaction (CO<sub>2</sub>RR) test.

In addition to the porous Cu samples, Cu foils were also tested in the CO<sub>2</sub>RR process for a comparison purpose. The surface of the Cu foil samples was polished by 400 grit silicon carbide paper prior to the tests.

#### 2.4. Product Analysis

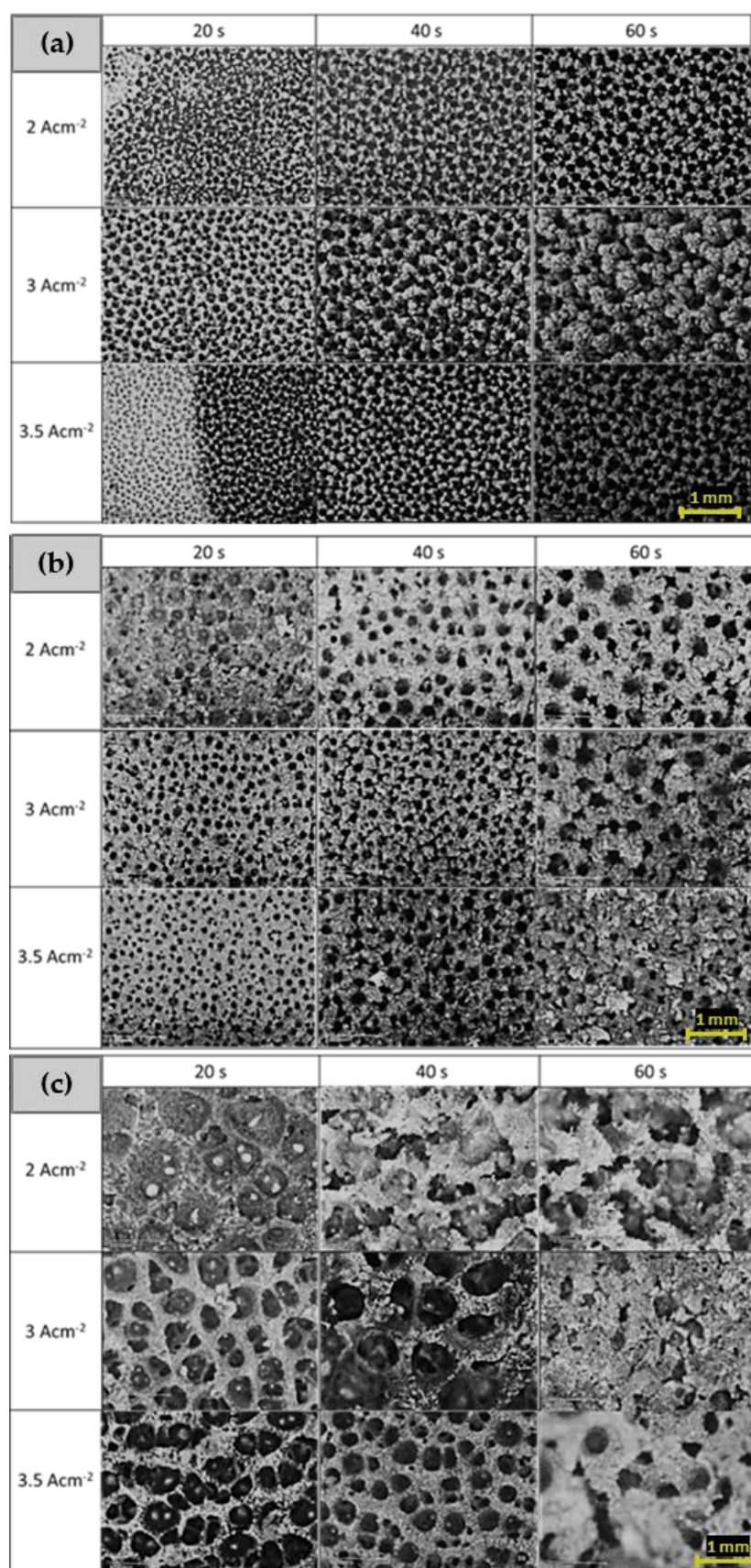
After running CO<sub>2</sub>RR, gas products were detected and analyzed online concurrently by GC. The accumulated amount of gas was calculated based on the average concentrations of gas products collected at 30 and 70 min of each run. To examine liquid products, if any, the electrolyte was collected for NMR analysis after tests were run for 70 min. Dimethyl sulfoxide (DMSO) was used as an internal standard, whereas deuterium oxide (D<sub>2</sub>O) was used as a solvent.

### 3. Results and Discussions

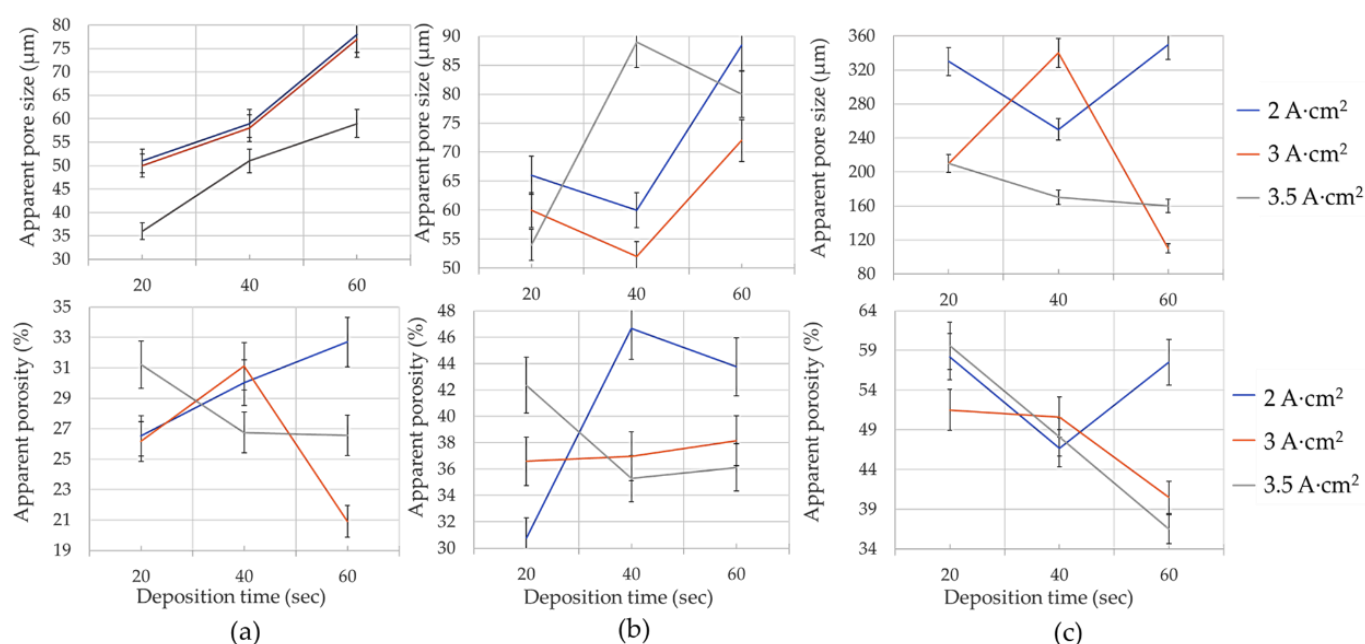
#### 3.1. Electrodeposition of Porous Copper

All 27 sets of the porous Cu samples were successfully deposited with uniform surface appearance. The morphology of the samples and correlations of process parameters and pore characteristics are presented in Figures 2 and 3, respectively. Figure 2a shows the morphology of the samples in group A, prepared by various applied current densities and deposition times. It is evidenced that the distribution of pore sizes as observed from the surface is rather uniform, and that both of the two parameters significantly affect the apparent porosity and apparent pore size observed at the surface. Particularly, the decrease of applied current and the increase of deposition time led to enlargement of apparent pore size. This may be attributed to slow rates of hydrogen evolution in conjunction with bubble coalescence in such conditions [5,35,36]. The effects of the two parameters on apparent porosity are however inconclusive, and the values of apparent porosity vary less significantly as compared to pore size.





**Figure 2.** Surface morphology of the Cu electrodeposits in group (a) A, (b) B, and (c) C, prepared by varying applied current densities and deposition times.



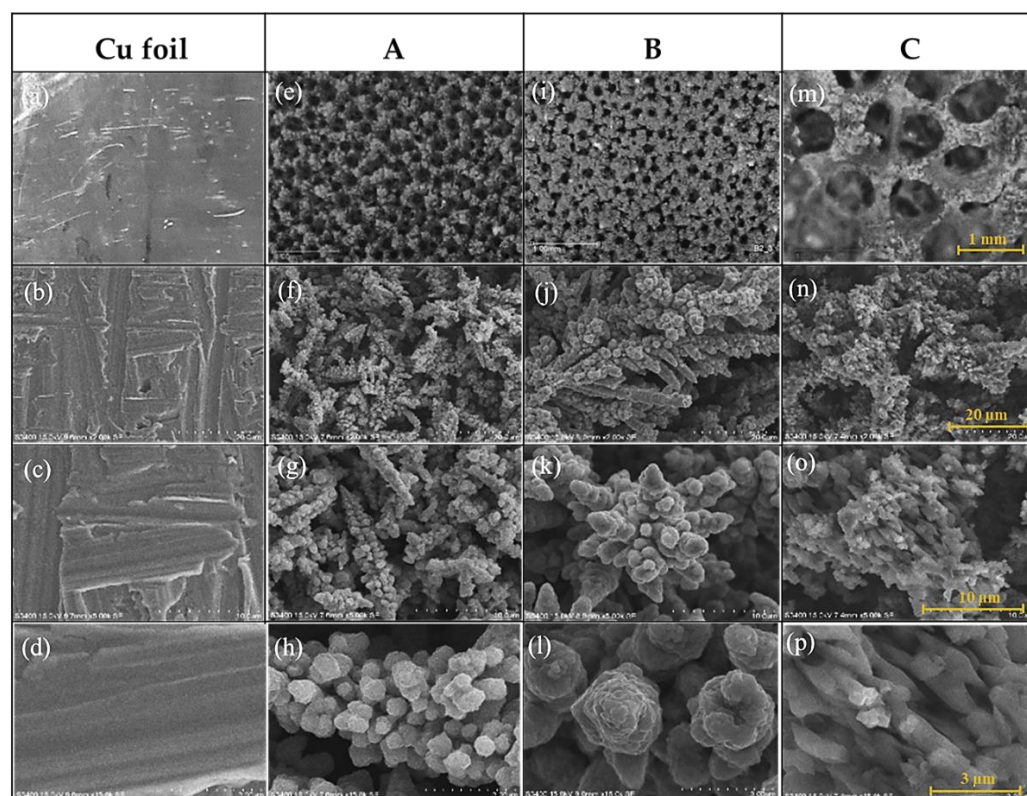
**Figure 3.** Apparent pore size and apparent porosity of the Cu electrodeposits in groups (a) A, (b) B, and (c) C.

Figure 2b shows the morphology of the samples in group B. Similar to those in group A, applied current density and deposition time appear to influence apparent pore size more than porosity. Overall, considering the same sets of plating parameters, the group B samples exhibit either similar or higher apparent pore size and apparent porosity as compared to group A samples. At first glance, this appears counter-intuitive, since the ratio of  $\text{H}_2\text{SO}_4$  (which contribute  $\text{H}^+$ ) and  $\text{Cu}_2\text{SO}_4$  is higher for group A. This may however imply that the group A samples comprise of a higher number of smaller-sized pores, in a nano regime, which were not clearly captured by image J software. Indeed, upon a closer examination using BET, it is found that the true surface area of the sample from group A is much higher than that from group B (Table 2), indicating a large number of nano-pores distributed along the struts of the porous Cu structure. The magnified microstructure of the group A sample (Figure 4), composing of clusters of sub-micron particulates and nano-pore in between each particulate, underlines this observation.

**Table 2.** Characteristics and properties of the porous Cu electrodes from groups A, B, and C, electrodeposited with 3 A/cm<sup>2</sup> for 40 s.

Characteristics	A	B	C
Apparent pore size (μm)	58	52	340
Apparent porosity (%)	31	37	51
BET surface area (m <sup>2</sup> /g)	19.56	4.00	3.75
Apparent density (g/cm <sup>3</sup> )	0.34	0.47	0.26
True porosity (%)	96.26	94.77	97.07
EDX Cu content (at.%)	89.0	87.2	71.3
EDX O content (at.%)	10.5	12.8	27.8

As shown in the micrographs of the samples in group C (Figure 2c), it is evident that their apparent pore size and apparent porosity are somewhat larger than those of the other two groups. This is clearly owed to the effect of HCl addition in the plating bath that promotes hydrogen generation and bubble coalescence. Although the effects of applied current and deposition time on the apparent pore size and apparent porosity are inconclusive, the increase of applied current and deposition time generally lead to reductions of apparent pore size and apparent porosity, especially for the relatively high applied current conditions.



**Figure 4.** Microstructure of Cu foil (a–d), and porous Cu deposits from groups A (e–h), B (i–l), and C (m–p), electrodeposited with 3 A/cm<sup>2</sup> for 40 s, presented at different magnifications.

The representative samples from the three groups, namely A, B, and C, that were electrodeposited with 3 A/cm<sup>2</sup> for 40 s, were characterized in more details, and their respective characteristics and properties are summarized in Figure 4 and Table 2. It is clear that bath compositions (A, B, and C) largely influence the developed porous structure of the Cu deposits. Not only are the samples from the three groups distinct in terms of apparent pore size and apparent porosity, but their detailed features of deposit nodules along the struts of the porous structure also appear to vary largely. Table 2 presents BET surface area, apparent pore size, apparent porosity, apparent density (determined from the coating mass and layer thickness), and true porosity. Overall, the true porosity obtained in this work falls in the range of the copper deposits' porosity obtained by the research of Shin et al. (93.30–97.77%) [4].

The group A sample is characterized by a structure with relatively high surface area, whereas the group B sample contains denser struts. The group C sample is unique with its relatively large pore size and strut size. It is also interesting to note that, based on a preliminary analysis of the coating surfaces using EDX, the oxygen content in the coatings are varied from one another, and significantly higher than that measured from the surface of the Cu foil counterpart (96.7 at.% Cu and 3.3 at.% O). While the presenting data of oxygen cannot be taken as absolute values, as oxygen is considered a light element for EDX analysis, and more advanced chemical analysis techniques would be required to determine the exact oxygen contents, it can be observed and qualitatively analyzed that the measured oxygen contents of the porous Cu samples deviate (increase) rather significantly compared to the Cu foil (Table 2). This suggests the role of porosity in promoting the absorption of chemical species and transformation of surface chemistry of the Cu deposits. Figure 5 shows XPS profiles of the porous Cu electrodes obtained after the CO<sub>2</sub>RR test sessions. The results indicate that the ratio of Cu and O contents of the group A, B, and C samples are 0.35, 0.31, and 0.45, respectively. The ratio of Cu<sup>+</sup>/Cu<sup>2+</sup> of these three sets of samples are 0.88, 0.24, and 0.84, respectively.



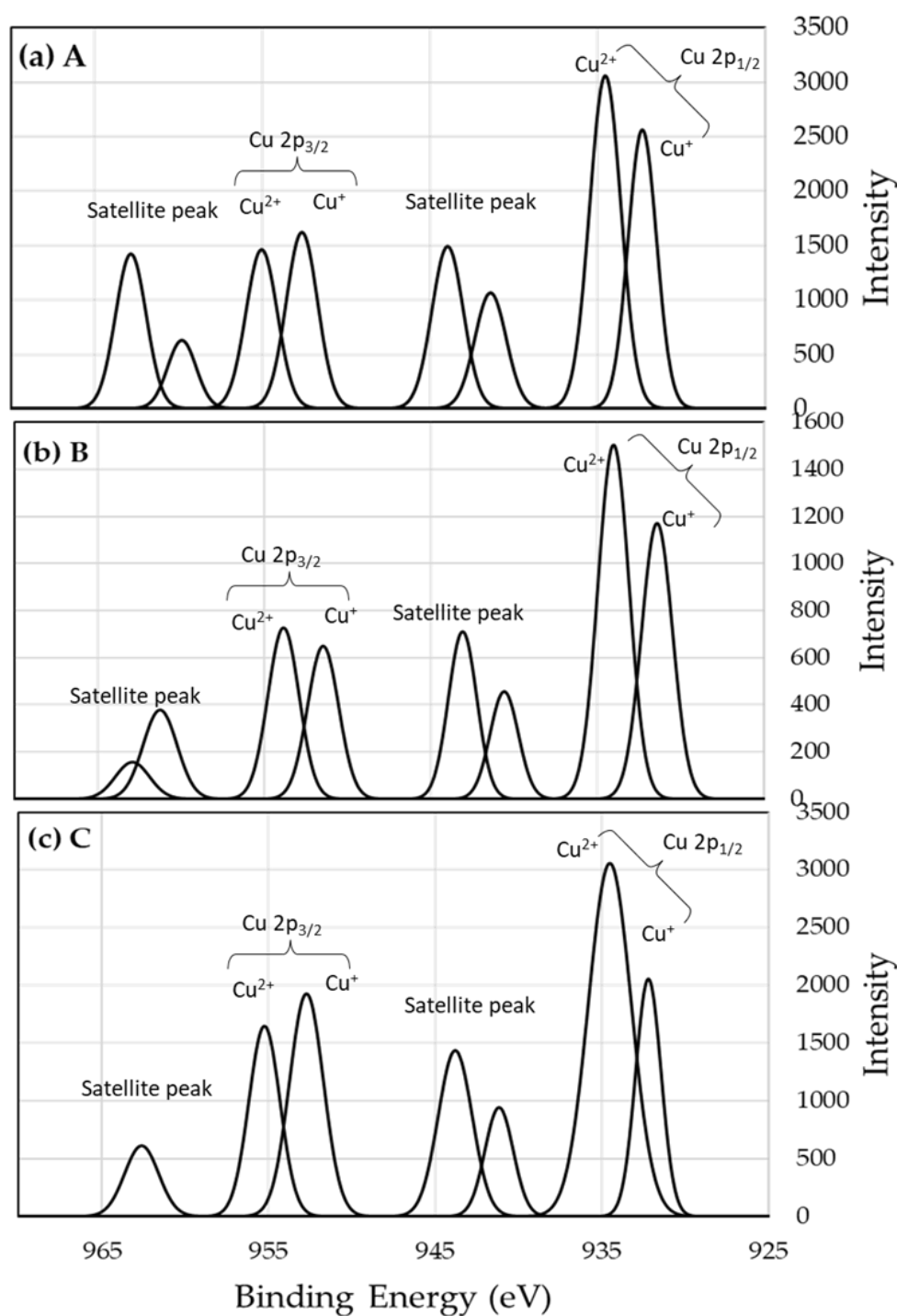


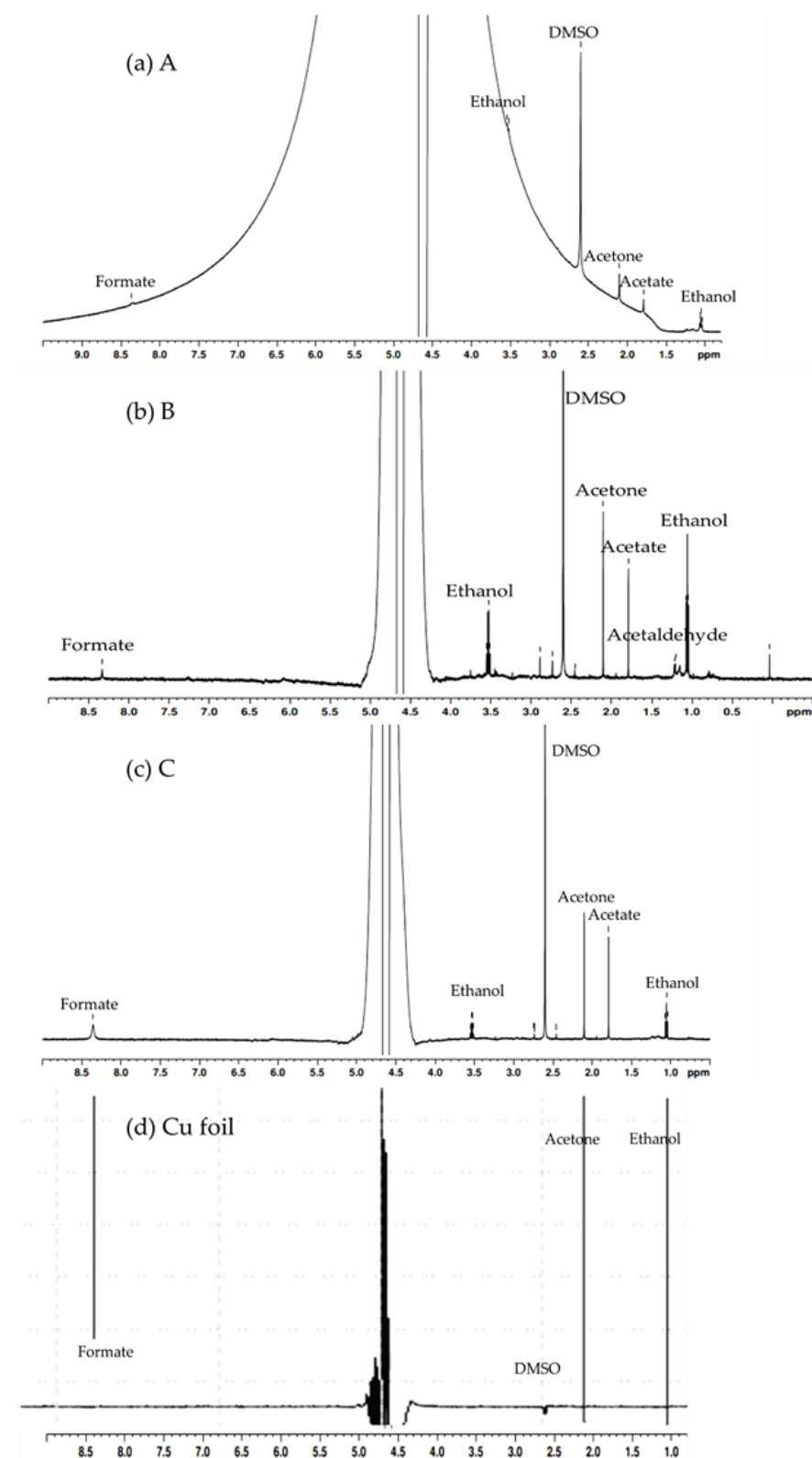
**Figure 5.** Representative XPS spectra of the porous Cu electrodes from groups (a) A, (b) B, and (c) C, electrodeposited with 3 A/cm<sup>2</sup> for 40 s, following the CO<sub>2</sub>RR experiments.

### 3.2. CO<sub>2</sub>RR Analysis

Table 3 shows the results of CO<sub>2</sub>RR tests of the porous Cu samples from groups A, B, and C, and the Cu foil, reported in terms of the chemical products' contents as detected by GC and NMR. Representative NMR spectra obtained from the study are shown in Figure 6. A single peak of DMSO, the internal standard, is present at 2.6 ppm. Acetate, acetone, and formate peaks are at 1.792, 2.103, and 8.363 ppm, respectively. Triple spikes at 1 ppm and quadruple spikes at 3.5 ppm represent ethanol. Acetaldehyde is detected with double spikes at 1.2 ppm. Figures 7 and 8 respectively present the rates of production



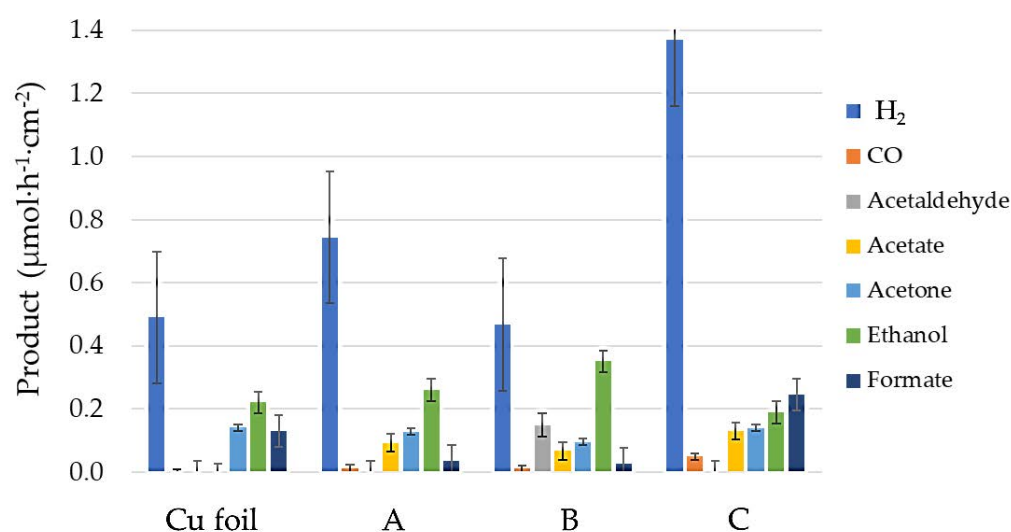
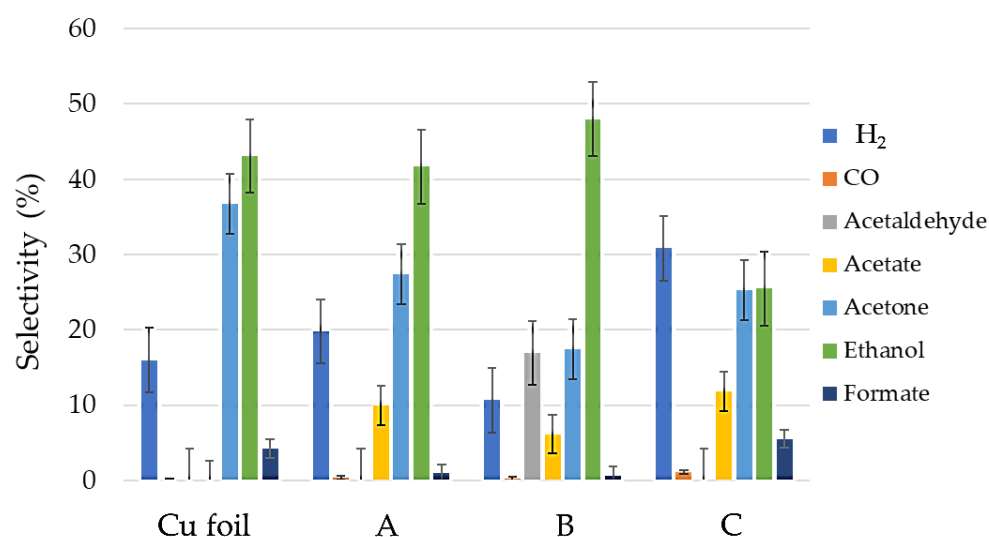
of the chemical products, and % selectivity is calculated by comparing a partial current density of a particular species to the sum of partial current densities of all detectable chemical products.



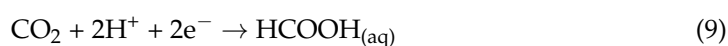
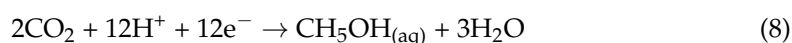
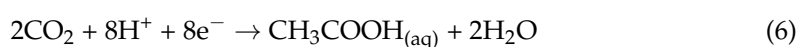
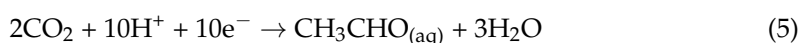
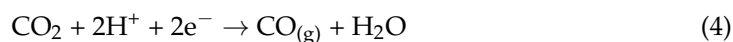
**Figure 6.** Representative NMR spectra obtained from the CO<sub>2</sub>RR experiments, using porous Cu samples from groups (a) A, (b) B, and (c) C, electrodeposited with 3 A/cm<sup>2</sup> for 40 s, and (d) the Cu foil as electrodes.

**Table 3.** Amounts of chemical products and reduction current density of CO<sub>2</sub>RR obtained from different groups of copper electrodes.

Sample	Reduction Current Density (mA/cm <sup>2</sup> )	Product (μmol)						
		Gas Product		Aqueous Product				
		H <sub>2</sub>	CO	CH <sub>3</sub> CHO	CH <sub>3</sub> COO <sup>−</sup>	CH <sub>3</sub> COCH <sub>3</sub>	CH <sub>3</sub> OH	HCOO <sup>−</sup>
Cu foil	−0.62	3.58	-	-	-	1.03	1.61	0.95
A	−4.11	5.42	0.09	-	0.68	0.94	1.90	0.26
B	−4.74	3.40	0.08	1.08	0.49	0.70	2.56	0.19
C	−4.40	9.98	0.36	-	0.95	1.02	1.38	1.79

**Figure 7.** Rate of production of the chemical products of CO<sub>2</sub>RR obtained from different groups of Cu electrodes, Cu foil and the porous Cu electrodes from groups A, B, and C, electrodeposited with 3 A/cm<sup>2</sup> for 40 s.**Figure 8.** Selectivity of the chemical products of CO<sub>2</sub>RR obtained from different groups of Cu electrodes, Cu foil and the porous Cu electrodes from groups A, B, and C, electrodeposited with 3 A/cm<sup>2</sup> for 40 s.

Generally, the mechanism pathway of the electrochemical conversion of CO<sub>2</sub> involves adsorption of CO<sub>2</sub> on an electrocatalytic surface and a transformation of CO<sub>2</sub> to a radical (CO<sub>2</sub><sup>•</sup>) and subsequently to an intermediate (\*CO) through electron and proton transfers. It is this intermediate that can be further transformed to different chemical products. The electrocatalysts, Cu in this case, would influence the reaction pathway, and hence the resulting intermediate species and final products, owing to their binding affinity to CO and different intermediates in the conversion processes. Considering the results in Figure 3, the chemical products and possible related cathodic reactions generated at the Cu electrodes under investigation include:



It can be observed that all porous Cu specimens provided relatively high current density, signifying a faster rate of reduction reaction, as compared to the Cu foil. For all types of Cu electrodes under consideration, the products comprised those in gas and liquid forms. H<sub>2</sub> was the major gas product found in all testing groups, whereas CO was detected only in the systems with porous Cu electrodes. The group C electrode in particular provided relatively high amounts of H<sub>2</sub> and CO, approximately 3–4 times higher than that of other porous Cu groups. Furthermore, whereas the Cu foil electrode provided acetone, ethanol and formate, the use of electrocatalytic porous Cu resulted in additional chemical products not found from the Cu foil system, including acetaldehyde and acetate. The group B sample, specifically, provided the highest reduction current density, and gave both acetaldehyde and acetate, and relatively high selectivity of ethanol compared to other testing electrodes. The group A electrode also yielded comparatively high selectivity of ethanol, but acetaldehyde was not detected from this system. The group C electrode, on the other hand, is unique in its relatively high production rate of formate, compared to the other sample groups.

From the results presented above, it is evidenced that the deposition of DHBT porous Cu influences both the electrochemical reduction rate of CO<sub>2</sub> and selectivity of species of chemical products developed from the CO<sub>2</sub>RR process. These improvements may stem from various factors related to the intricate structures of the porous Cu electrodes, as follows: (i) porous structures appear to promote the absorption of chemical species, including oxygen as noted previously. As demonstrated by Dutta et al. [2], Lv et al. [12], and Nguyen-Phan et al. [37], the surface of copper oxide thus formed can play a role in promoting the catalytic activity, owing to the development of a large number of active sites and roughening of the surface, following reduction of the oxide phase over the course of CO<sub>2</sub>RR. Furthermore, the XPS analysis (Figure 5) signifies that porous Cu electrodes of different morphologies exhibit a variation of oxidation states of Cu on the surface (i.e., Cu<sup>+</sup>/Cu<sup>2+</sup>). The oxidation states of Cu are known to influence preferential formations of intermediates and hence affect the CO<sub>2</sub> reduction pathways and promote selectivity [30,34,38]. In addition, (ii) the intricate structure of the porous Cu electrodes may enhance dynamic diffusion of the dissolved gas to provide increasing CO<sub>2</sub> concentration at the catalytic electrode–electrolyte interface [12]. Temporal trapping of gaseous intermediates, e.g., CO,

could also be induced inside the pores [2]. Furthermore, the high porosity of the porous Cu provides high surface areas and hence large active sites for the electrodes. Correspondingly, the retention time for CO<sub>2</sub>RR could be effectively enlarged. Unlike H<sub>2</sub>, CO and formate, which require minimal amounts of electron transfers (1–2 electrons) to generate, larger hydrocarbon molecules such as acetate, acetaldehyde and ethanol require many more electron transfers (8, 10, and 12 electrons, respectively), making them challenging to produce from the CO<sub>2</sub>RR process generally. Yet, these three chemical products were detected from the systems with the porous Cu electrodes investigated herein with relatively high selectivity.

Examining more closely, electrode B appears to exhibit the best performance in terms of the reduction rate and a variety of the chemical products, albeit the true surface area of electrode B is somewhat lower than that of electrode A. This result thus underlines that surface area is not the only primary factor underlining the good performance of the electrode, but rather other influences such as surface morphology (i.e., cluster of a berry-like structure of A vs. fern-like morphology of B) and surface chemistry (e.g., alternation of surface chemistry by adsorbed oxygen and oxidation states) also play important roles. Further examination and analysis will thus be required to gain insights on the contribution of important factors that lead to the enhancement of electrode performance observed herein, along with understanding of the suitable applied overpotentials and other control parameters to optimally induce CO<sub>2</sub>RR for respective porous Cu electrodes.

#### 4. Conclusions

Porous Cu samples were fabricated by the dynamic hydrogen bubble template (DHBT) method and investigated for their uses in the electrochemical CO<sub>2</sub> reduction reaction (CO<sub>2</sub>RR). The composition of Cu plating baths largely influenced pore size and microstructure of the porous Cu samples; the bath with low concentrations of copper salt gave deposits with relatively large surface area, whereas the addition of hydrochloric acid granted larger pore sizes. Applied current density and deposition time were shown to affect the porous Cu's characteristics in different ways depending on the bath compositions. Compared to the Cu foil, porous Cu as CO<sub>2</sub>RR electrodes generally provided relatively high reduction current density. The porous Cu electrode from group B with fern-like morphology, in particular, provided the highest reduction current density among others, and gave acetaldehyde and acetate, and relatively high amounts of ethanol as liquid products, along with hydrogen and carbon monoxide as gas products. That porous structures of the Cu electrodes promoted the electrochemical reduction rate of CO<sub>2</sub>, and generation of various chemical products could be due to increased absorption of chemical species, particularly oxygen, enhancements of CO<sub>2</sub> concentration at the catalytic electrode surface, and the retention time for the reduction reactions.

**Author Contributions:** Conceptualization and methodology, Y.B. and J.P.; investigation, J.D.; formal analysis, J.D., O.C., J.P. and D.N.T.; writing—original draft preparation, J.D.; writing—review and editing, Y.B.; supervision and funding acquisition, P.P. All authors have read and agreed to the published version of the manuscript.

**Funding:** This research was funded by the Royal Golden Jubilee Ph.D. Program (RGJ-Ph.D. Program), Thailand Science Research and Innovation (CAT-REAC industrial project (RDG6250033)), and the Malaysia–Thailand Joint Authority (MTJA).

**Acknowledgments:** This study was financially supported by the Royal Golden Jubilee Ph.D. Program (RGJ-Ph.D. Program (PHD/0126/2560)), Thailand Science Research and Innovation (CAT-REAC industrial project (RDG6250033)), and the Malaysia–Thailand Joint Authority (MTJA). The authors also gratefully acknowledge the technical staff at the Center of Excellence on Catalysis and Catalytic Reaction Engineering for their support.

**Conflicts of Interest:** The authors declare no conflict of interest.



## References

- Li, M.; Wang, J.; Li, P.; Chang, K.; Li, C.; Wang, T.; Jiang, B.; Zhang, H.; Liu, H.; Yamauchi, Y.; et al. Mesoporous palladium–copper bimetallic electrodes for selective electrocatalytic reduction of aqueous CO<sub>2</sub> to CO. *J. Mater. Chem. A* **2016**, *4*, 4776–4782. [\[CrossRef\]](#)
- Dutta, A.; Rahaman, M.; Luedi, N.C.; Mohos, M.; Broekmann, P. Morphology Matters: Tuning the Product Distribution of CO<sub>2</sub> Electroreduction on Oxide-Derived Cu Foam Catalysts. *ACS Catal.* **2016**, *6*, 3804–3814. [\[CrossRef\]](#)
- Pestryakov, A.; Petranovskii, V.; Pfänder, N.; Knop-Gericke, A. Supported foam–copper catalysts for methanol selective oxidation. *Catal. Commun.* **2004**, *5*, 777–781. [\[CrossRef\]](#)
- Shin, H.-C.; Liu, M. Copper Foam Structures with Highly Porous Nanostructured Walls. *Chem. Mater.* **2004**, *16*, 5460–5464. [\[CrossRef\]](#)
- Najdovski, I. The Electrochemical Fabrication of Porous Bimetallic Structures and Their Applications in Catalysis and Sensing. Ph.D. Thesis, RMIT University, Melbourne, Australia, 2013.
- Huang, Y.; Handoko, A.D.; Hirunsit, P.; Yeo, B.S. Electrochemical Reduction of CO<sub>2</sub> Using Copper Single-Crystal Surfaces: Effects of CO\* Coverage on the Selective Formation of Ethylene. *ACS Catal.* **2017**, *7*, 1749–1756. [\[CrossRef\]](#)
- Rasul, S.; Pugniant, A.; Xiang, H.; Fontmorin, J.-M.; Yu, E.H. Low cost and efficient alloy electrocatalysts for CO<sub>2</sub> reduction to formate. *J. CO<sub>2</sub> Util.* **2019**, *32*, 1–10. [\[CrossRef\]](#)
- Chen, Y.; Li, C.W.; Kanan, M.W. Aqueous CO<sub>2</sub> Reduction at Very Low Overpotential on Oxide-Derived Au Nanoparticles. *J. Am. Chem. Soc.* **2012**, *134*, 19969–19972. [\[CrossRef\]](#) [\[PubMed\]](#)
- Min, S.; Yang, X.; Lu, A.-Y.; Tseng, C.-C.; Hedhili, M.N.; Li, L.-J.; Huang, K.-W. Low overpotential and high current CO<sub>2</sub> reduction with surface reconstructed Cu foam electrodes. *Nano Energy* **2016**, *27*, 121–129. [\[CrossRef\]](#)
- Sen, S.; Liu, D.; Palmore, G.T.R. Electrochemical Reduction of CO<sub>2</sub> at Copper Nanofoams. *ACS Catal.* **2014**, *4*, 3091–3095. [\[CrossRef\]](#)
- Kas, R.; Hummadi, K.K.; Kortlever, R.; De Wit, P.; Milbrat, A.; Luiten-Olieman, M.W.J.; Benes, N.E.; Koper, R.K.M.T.M.; Mul, G. Three-dimensional porous hollow fibre copper electrodes for efficient and high-rate electrochemical carbon dioxide reduction. *Nat. Commun.* **2016**, *7*, 10748. [\[CrossRef\]](#)
- Lv, J.; Jouny, M.; Luc, W.; Zhu, W.; Zhu, J.; Jiao, F. A Highly Porous Copper Electrocatalyst for Carbon Dioxide Reduction. *Adv. Mater.* **2018**, *30*, e1803111. [\[CrossRef\]](#)
- Zhu, P.; Wu, Z.; Zhao, Y. Hierarchical porous Cu with high surface area and fluid permeability. *Scr. Mater.* **2019**, *172*, 119–124. [\[CrossRef\]](#)
- Cao, C.; Cheng, J. Fabrication of robust surfaces with special wettability on porous copper substrates for various oil/water separations. *Chem. Eng. J.* **2018**, *347*, 585–594. [\[CrossRef\]](#)
- Michailidis, N.; Stergioudi, F.; Seventekidis, P.; Tsouknidas, A.; Sagris, D. Production of porous copper with high surface area for efficient water purification. *CIRP J. Manuf. Sci. Technol.* **2016**, *13*, 85–89. [\[CrossRef\]](#)
- Rehman, T.-U.; Ali, H.M. Experimental investigation on paraffin wax integrated with copper foam based heat sinks for electronic components thermal cooling. *Int. Commun. Heat Mass Transf.* **2018**, *98*, 155–162. [\[CrossRef\]](#)
- Liu, Y.; Zhou, W.; Lin, Y.; Chen, L.; Chu, X.; Zheng, T.; Wan, S.; Lin, J. Novel copper foam with ordered hole arrays as catalyst support for methanol steam reforming microreactor. *Appl. Energy* **2019**, *246*, 24–37. [\[CrossRef\]](#)
- Plowman, B.J.; Jones, L.A.; Bhargava, S.K. Building with bubbles: The formation of high surface area honeycomb-like films via hydrogen bubble templated electrodeposition. *Chem. Commun.* **2015**, *51*, 4331–4346. [\[CrossRef\]](#)
- Zhang, H.; Ye, Y.; Shen, R.; Ru, C.; Hu, Y. Effect of Bubble Behavior on the Morphology of Foamed Porous Copper Prepared via Electrodeposition. *J. Electrochem. Soc.* **2013**, *160*, D441–D445. [\[CrossRef\]](#)
- Nguyen, T.; Boudard, M.; Carmezim, M.; Montemor, F. Hydrogen bubbling-induced micro/nano porous MnO<sub>2</sub> films prepared by electrodeposition for pseudocapacitor electrodes. *Electrochim. Acta* **2016**, *202*, 166–174. [\[CrossRef\]](#)
- Berkesi, K. Electrodeposited iron-based nanofoams as precursors for transducers. *J. Phys. Conf. Ser.* **2017**, *939*, 012037. [\[CrossRef\]](#)
- Yang, K.D.; Ko, W.R.; Lee, J.H.; Kim, S.J.; Lee, H.; Lee, M.H.; Nam, K.T. Morphology-Directed Selective Production of Ethylene or Ethane from CO<sub>2</sub> on a Cu Mesopore Electrode. *Angew. Chem. Int. Ed.* **2017**, *56*, 796–800. [\[CrossRef\]](#) [\[PubMed\]](#)
- Padilla, M.; Baturina, O.; Gordon, J.P.; Artyushkova, K.; Atanassov, P.; Serov, A. Selective CO<sub>2</sub> electroreduction to CH<sub>4</sub> on porous Cu films synthesized by sacrificial support method. *J. CO<sub>2</sub> Util.* **2017**, *19*, 137–145. [\[CrossRef\]](#)
- Jhong, H.-R.; Ma, S.; Kenis, P.J. Electrochemical conversion of CO<sub>2</sub> to useful chemicals: Current status, remaining challenges, and future opportunities. *Curr. Opin. Chem. Eng.* **2013**, *2*, 191–199. [\[CrossRef\]](#)
- Hori, Y. Electrochemical CO<sub>2</sub> Reduction on Metal Electrodes. In *Modern Aspects of Electrochemistry*; Vayenas, C.G., White, R.E., Gamboa-Aldeco, M.E., Eds.; Springer: New York, NY, USA, 2008; pp. 89–189.
- Kuhl, K.P.; Cave, E.R.; Abram, D.N.; Jaramillo, T.F. New insights into the electrochemical reduction of carbon dioxide on metallic copper surfaces. *Energy Environ. Sci.* **2012**, *5*, 7050–7059. [\[CrossRef\]](#)
- Pérez-Fortes, M.; Schöneberger, J.C.; Boulamanti, A.; Tzimas, E. Methanol synthesis using captured CO<sub>2</sub> as raw material: Techno-economic and environmental assessment. *Appl. Energy* **2016**, *161*, 718–732. [\[CrossRef\]](#)
- Hirunsit, P.; Soodsawang, W.; Limtrakul, J. CO<sub>2</sub> Electrochemical Reduction to Methane and Methanol on Copper-Based Alloys: Theoretical Insight. *J. Phys. Chem. C* **2015**, *119*, 8238–8249. [\[CrossRef\]](#)
- Hatsukade, T.; Kuhl, K.P.; Cave, E.R.; Abram, D.N.; Jaramillo, T.F. Insights into the electrocatalytic reduction of CO<sub>2</sub> on metallic silver surfaces. *Phys. Chem. Chem. Phys.* **2014**, *16*, 13814–13819. [\[CrossRef\]](#)

30. Lee, S.Y.; Jung, H.; Kim, N.-K.; Oh, H.-S.; Min, B.K.; Hwang, Y.J. Mixed Copper States in Anodized Cu Electrocatalyst for Stable and Selective Ethylene Production from CO<sub>2</sub> Reduction. *J. Am. Chem. Soc.* **2018**, *140*, 8681–8689. [[CrossRef](#)]
31. Wang, X.; Klingan, K.; Klingenhof, M.; Möller, T.; de Araújo, J.F.; Martens, I.; Bagger, A.; Jiang, S.; Rossmeisl, J.; Dau, H.; et al. Morphology and mechanism of highly selective Cu(II) oxide nanosheet catalysts for carbon dioxide electroreduction. *Nat. Commun.* **2021**, *12*, 1–12. [[CrossRef](#)]
32. Li, C.; Kanan, M.W. CO<sub>2</sub> Reduction at Low Overpotential on Cu Electrodes Resulting from the Reduction of Thick Cu<sub>2</sub>O Films. *J. Am. Chem. Soc.* **2012**, *134*, 7231–7234. [[CrossRef](#)]
33. Ren, D.; Deng, Y.; Handoko, A.D.; Chen, C.S.; Malkhandi, S.; Yeo, B.S. Selective Electrochemical Reduction of Carbon Dioxide to Ethylene and Ethanol on Copper(I) Oxide Catalysts. *ACS Catal.* **2015**, *5*, 2814–2821. [[CrossRef](#)]
34. Xiao, H.; Iii, W.A.G.; Cheng, T.; Liu, Y. Cu metal embedded in oxidized matrix catalyst to promote CO<sub>2</sub> activation and CO dimerization for electrochemical reduction of CO<sub>2</sub>. *Proc. Natl. Acad. Sci. USA* **2017**, *114*, 6685. [[PubMed](#)]
35. Daiyan, R.; Lu, X.; Ng, Y.H.; Amal, R. Highly Selective Conversion of CO<sub>2</sub> to CO Achieved by a Three-Dimensional Porous Silver Electrocatalyst. *ChemistrySelect* **2017**, *2*, 879–884. [[CrossRef](#)]
36. Niu, J.; Liu, X.; Xia, K.; Xu, L.; Xu, Y.; Fang, X.; Lu, W. Effect of electrodeposition parameters on the morphology of three-dimensional porous copper foams. *Int. J. Electrochem. Sci.* **2015**, *10*, 7331–7340.
37. Nguyen-Phan, T.-D.; Wang, C.; Marin, C.M.; Zhou, Y.; Stavitski, E.; Popczun, E.J.; Yu, Y.; Xu, W.; Howard, B.H.; Stuckman, M.Y.; et al. Understanding three-dimensionally interconnected porous oxide-derived copper electrocatalyst for selective carbon dioxide reduction. *J. Mater. Chem. A* **2019**, *7*, 27576–27584. [[CrossRef](#)]
38. Chou, T.-C.; Chang, C.-C.; Yu, H.-L.; Yu, W.-Y.; Dong, C.-L.; Velasco-Vélez, J.-J.; Chuang, C.-H.; Chen, L.-C.; Lee, J.-F.; Chen, J.-M.; et al. Controlling the Oxidation State of the Cu Electrode and Reaction Intermediates for Electrochemical CO<sub>2</sub> Reduction to Ethylene. *J. Am. Chem. Soc.* **2020**, *142*, 2857–2867. [[CrossRef](#)]